

## Article

# Metasomatism by Boron-Rich Fluids along Permian Low-Angle Normal Faults (Central Southern Alps, N Italy)

Stefano Zanchetta \*, Sofia Locchi \*, Gregorio Carminati, Manuel Mancuso, Chiara Montemagni and Andrea Zanchi

Department of Earth and Environmental Sciences, University of Milano Bicocca, Piazza della Scienza 1, 20126 Milano, Italy; carminati.gregorio@gmail.com (G.C.); manuel.mancuso221291@gmail.com (M.M.); chiara.montemagni@unimib.it (C.M.); andrea.zanchi@unimib.it (A.Z.)

\* Correspondence: stefano.zanchetta@unimib.it (S.Z.); s.locchi@campus.unimib.it (S.L.)

**Abstract:** Low-Angle Normal Faults (LANFs) represent in the central Southern Alps area (N Italy) the main structures along which the Variscan basement is in contact with the Upper Carboniferous–Permian volcanic-sedimentary succession. Tourmalinites frequently occur along LANFs, usually replacing former cataclases. The mineralogy and chemical composition of tourmalinites point to a metasomatic origin. LANFs, together with high-angle faults, controlled the opening of the Permian Orobic Basin and likely acted as a preferred pathway for hydrothermal fluids that triggered the Boron-metasomatism. Along the Aga-Vedello LANF, tourmalinites appear to have formed after the cessation of fault activity, as no brittle post-metasomatism deformation overprint has been observed. These relationships suggest that the circulation of B-rich fluids occurred after the opening of the Orobic Basin that is broadly constrained to the Early Permian. At the same time, ca. 285–270 Ma, a strong magmatic activity affected all the Southern Alps, ranging in composition from mafic to acidic rocks and from intrusions at deep crustal levels to effusive volcanic products. The Early Permian magmatism was likely the source of the late-stage hydrothermal fluids that formed the tourmalinites. The same fluids could also have played a significant role in the formation of the Uranium ore deposit of the Novazza-Vedello mining district, as the ore bodies in the Vedello valley are concentrated along the basement-cover contact.

**Keywords:** Low-Angle Normal Faults; Boron-metasomatism; tourmalinites; Orobic Basin



**Citation:** Zanchetta, S.; Locchi, S.; Carminati, G.; Mancuso, M.; Montemagni, C.; Zanchi, A. Metasomatism by Boron-Rich Fluids along Permian Low-Angle Normal Faults (Central Southern Alps, N Italy). *Minerals* **2022**, *12*, 404. <https://doi.org/10.3390/min12040404>

Academic Editors: Manuel Roda and Jean-Marc Lardeaux

Received: 14 February 2022

Accepted: 23 March 2022

Published: 25 March 2022

**Publisher's Note:** MDPI stays neutral with regard to jurisdictional claims in published maps and institutional affiliations.



**Copyright:** © 2022 by the authors. Licensee MDPI, Basel, Switzerland. This article is an open access article distributed under the terms and conditions of the Creative Commons Attribution (CC BY) license (<https://creativecommons.org/licenses/by/4.0/>).

## 1. Introduction and Geological Setting

Immediately after the late stages of the Variscan orogeny, an episode of crustal extension starting in the Early Permian affected the Adria passive margin. Traces of these events are now preserved in the geological record of the central Southern Alps [1–6]. During the Alpine shortening, favorably oriented normal faults inherited from Permian tectonics [7–9] were re-activated and played an important role, being frequently inverted as south-verging thrusts. Despite the pervasive Alpine overprint, several portions of the Permian structures are still well preserved, displaying their original structural features. Among these, Low-Angle Normal Faults (LANFs) and detachment systems [9–11] are of particular interest as they provide insights into the tectonic framework that characterized the Early Permian crustal extension in the present-day central Southern Alps (cSA) area. This extensional phase that interested a very large area, from the Southern Alps to Central Europe, was not only responsible for the development of intracontinental basins [12] but was also related to a diffuse magmatic activity at different crustal levels and HT metamorphism [13–17]. The magmatic activity resulted in the emplacement of gabbro to gabbro-diorite bodies at the lower crust-mantle transition [13,18–21], emplacement of intermediate to acidic intrusive complexes at mid to shallow crustal levels [22–24] and, finally, volcanic and volcanoclastic products above the Upper Carboniferous–Lower Permian (?) Variscan non-conformity [14,25–28]. The interplay between tectonics, sedimentation, and magmatism during the Early Permian extensional phase is well documented in Central Europe [12],

whereas the Alpine tectonics overprint has since hampered its complete reconstruction and interpretation in the frame of the collapse of the late Variscan orogen in the cSA area [25–27]. Recent studies outlined that several parts of the Early Permian fault network are still well-preserved in the cSA [9–11,29] and offer the opportunity to give insights into the tectonic framework that marked the transition from the end of the Variscan orogeny to the Early Permian extension.

In this paper, we document a well preserved Early Permian LANF cropping out between the Ambria and Vedello valleys (SO). The area is well known also because it was explored between 1950 and 1970 in search of Uranium ores that were partially exploited between 1979 and 1982 [25,30,31]. The fault plane is characterized by cataclasites of variable thickness, mainly derived from comminution of the Permian cover rocks (the Vedello Conglomerate Auct. [32]), that were later impregnated by Boron-rich fluids responsible for the precipitation of tourmalinites [9,33–35]. In order to characterize this fault from a structural point of view, we performed detailed geological mapping at a scale comprised of between 1:100 and 1:10,000, accompanied by outcrop sampling, microstructural analyses, and mineral chemistry characterization of tourmalinites.

The cSA are a fold-and-thrust belt [8,36,37] that involves a polymetamorphic basement with metamorphism of Variscan age [38,39] and its Upper Carboniferous to Cenozoic sedimentary cover (Figure 1). During the Alpine orogenic event, significant crustal shortening was accommodated by thrusting and folding at very low-grade metamorphic conditions [40]. The main tectonic transport direction was toward SE with basement units that were stacked southward onto the Permian-Mesozoic cover [8,36,41–44]. In particular, in the northern area of the belt, the Orobic-Gallinera Thrust System occurs, stacking the Variscan basement on the Permian-Mesozoic succession of the northern portion of the Orobic Anticlines included in a set of ENE-WSW dextral en-échelon anticlines. Here, the basement and the Carboniferous to Lower Triassic successions crop out between the Orobic-Porcile-Gallinera Thrust System to the north and the Valtorta-Valcanale Fault to the south, where imbricated Triassic carbonates are dominant (Figure 1).

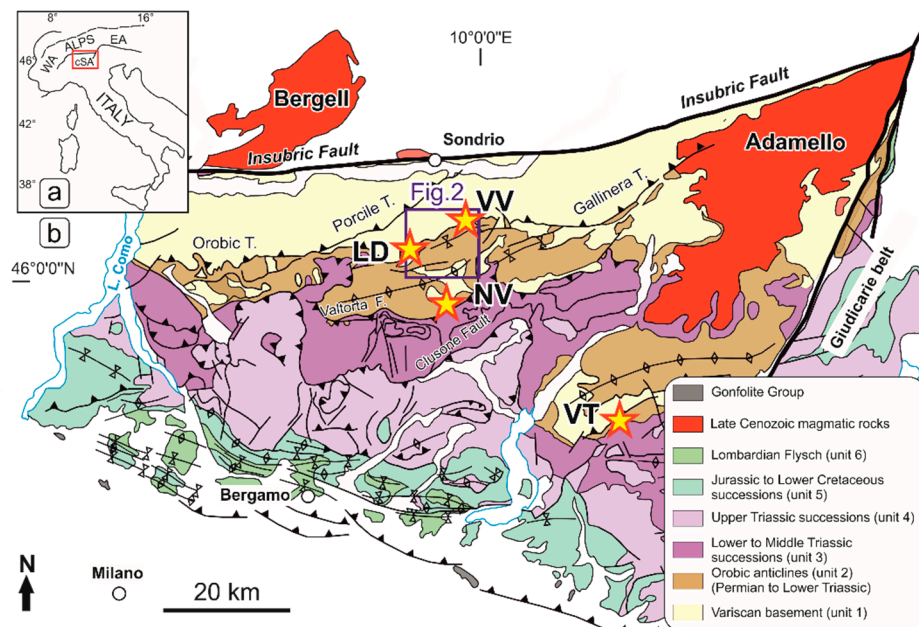


**Figure 1.** Tectonic scheme of the cSA, modified after [8]. The localities of tourmalinite occurrences are highlighted with yellow stars. LD: Lago del Diavolo-Mt. Aga; NV: Novazza Uranium ore deposit; VT: Val Trompia tourmalinites; VV: Val Vedello Uranium ore deposit. The extent of Figure 2 is reported.

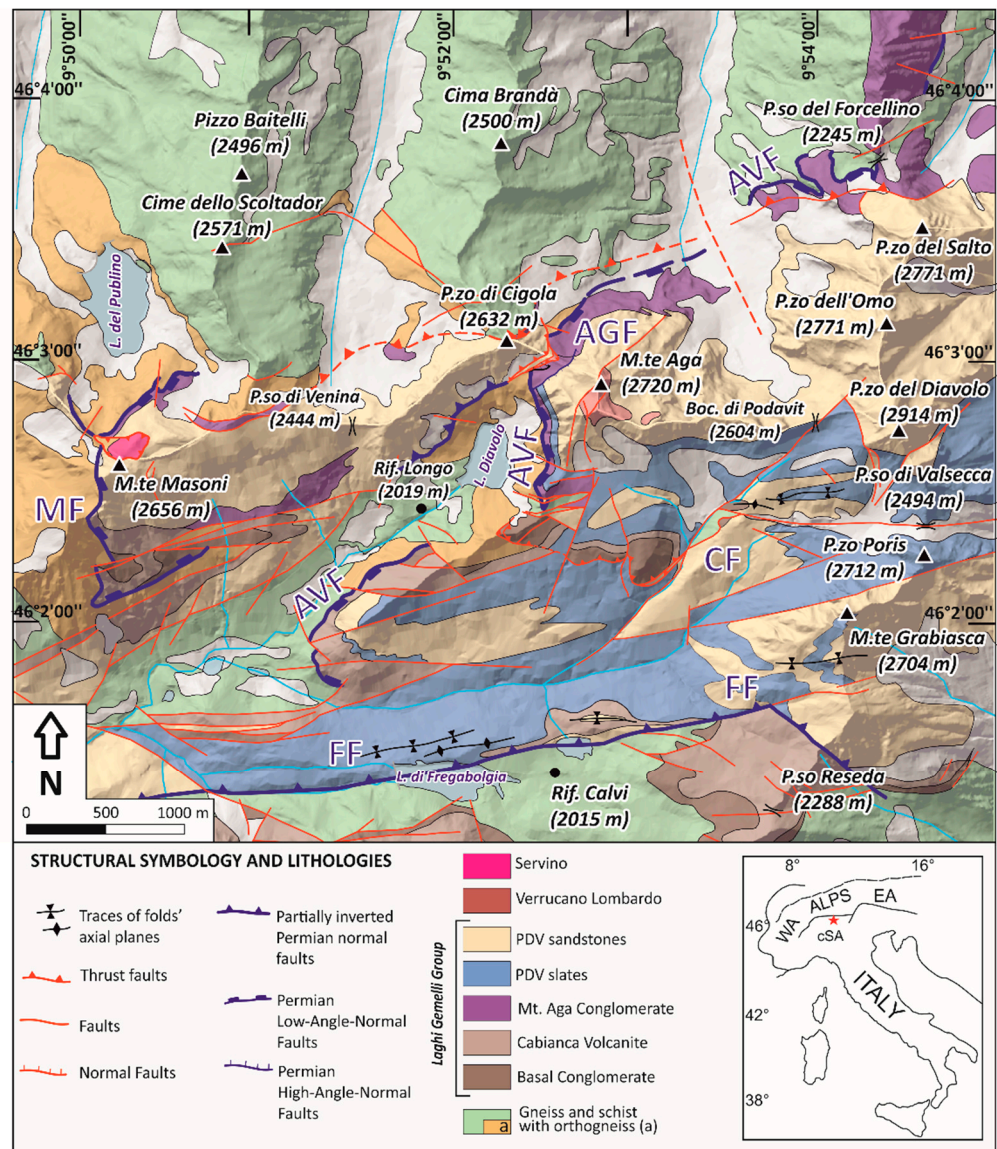


**Figure 2.** Simplified geological maps of the upper Brembana and Vedello valleys displaying the traces of the Aga-Vedello (AVF) and Masoni (MF) LANFs. AGF: Aga Growth Fault; CF: Camisana Fault; FF: Fregaborgia Fault. The Forcellino Pass is in the NE corner of the map. Modified from [9].

The Upper Carboniferous to Upper Permian sedimentary successions of the cSA are chiefly exposed [25,28] in the Orobic Anticlines. These antiformal structures almost correspond to the original extension of Permian basins, namely, from west to east, the Orobic, Boario, Collio, Tione, Tregiovo, Forni-Avoltri, and Pramollo Basins. The Upper Carboniferous—Permian succession of the cSA is characterized by the occurrence of two major sedimentary systems, i.e., the older terrigenous and volcanic units of the Laghi Gemelli Group [25,27,28], and a younger succession, consisting of the Upper Permian continental red beds of the Verrucano Lombardo. This unit is separated from the underlying Laghi Gemelli Group by an angular unconformity throughout the entire cSA area. The Lower Permian units are, from bottom to top: the up to 100 m thick Basal Conglomerate, covered by the ca. 800 m thick Monte Cabianca Vulcanite (CBV) in the study area, including large ignimbrite sheets (284 to 270 Ma [45]). The CBV is covered by the Pizzo del Diavolo Formation (PDV) which consists, in the central part of the Orobic Basin, of coarse-grained proximal conglomerates (Mt. Aga Conglomerate, AC, to the north and Val Sanguigno Conglomerate to the south), passing to fine-grained deposits (volcaniclastic sandstones

and dark mudstones) in the depocentral area of the basin. Tetrapods' footprints occurring within slates of the Pizzo del Diavolo area suggest a late most Kungurian age [46,47]. On the base of stratigraphic and tectonic evidence, the succession of the Laghi Gemelli Group is interpreted to have formed in an intracontinental fault-controlled basin developed in semi-arid conditions, strongly recalling the present-day Basin and Range Province [27]. Red sandstone and conglomerates of the Verrucano Lombardo (Lopingian) were deposited above an angular unconformity, testifying for tectonic activity and deep erosion of the Laghi Gemelli Group during the Middle-Late Permian [27,48].

The Orobic basin stratigraphy and architecture reflect Permian syn-depositional tectonic activity, associated with the development of E-W oriented faults and related facies belts [25,48]. The northern boundary of this basin is defined by the Mt. Aga Conglomerate overlying the Variscan basement along the Aga-Vedello Low-Angle Normal Fault (LANF) that documents, together with the Masoni LNF, the Early Permian extension [9] (Figure 2). This low angle fault system interacts with high angle normal faults active in a syn-sedimentary context during the deposition of the base of the PDV, where soft-sediment deformations at very shallow levels produced mesoscopic structures possibly related to seismic shaking [9,49]. This tectonic setting generated asymmetric half-grabens deepening toward the basins depocenters, along ENE-WSW oriented master faults. Fault planes of the described Permian fault system are often decorated by cryptocrystalline to aphanitic tourmalinites that impregnate cataclasites formed along the basement-cover fault contact [9,33–35]. Tourmalinites were likely formed due to hydrothermal fluid circulation associated with the emplacement of Permian magmatic bodies in the shallow crust [35]. Such magmatic bodies also occur in the Trompia Valley district (central Southern Alps), where the spatial relationship between tourmalinized faults and upper Palaeozoic granitoid intrusions were described [50–52].

## 2. Materials and Methods

Fieldwork and structural analysis of the fault architecture (Figures 3 and 4) were mainly conducted during 2018 and 2019 in the frame of the Master's Degree thesis of M. Mancuso and G. Carminati.

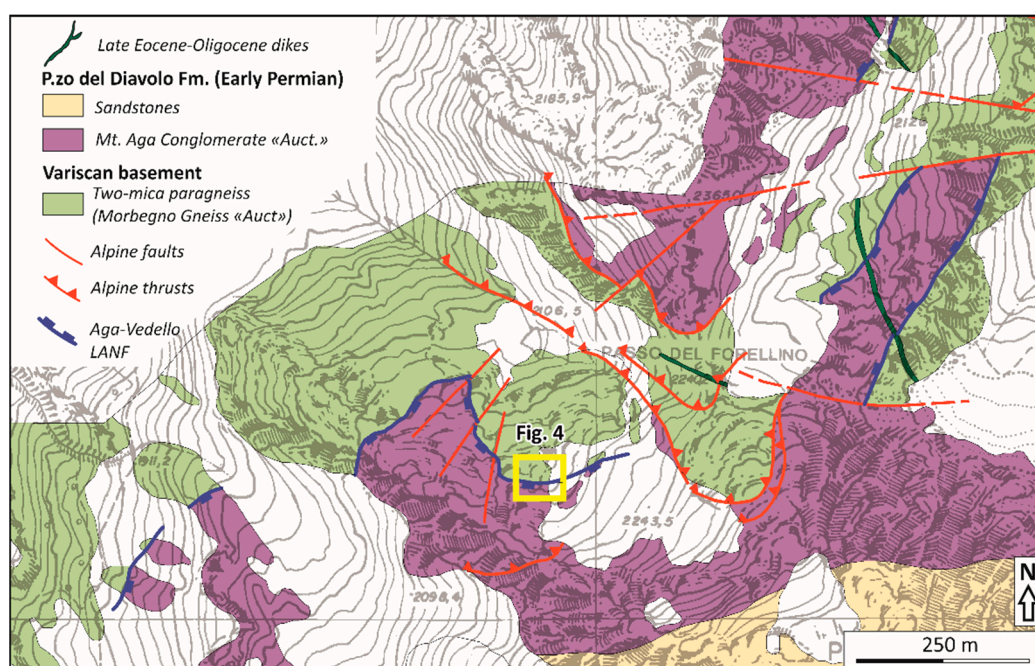


**Figure 3.** Geological map of the Forcellino Pass area. Parts of the Permian LNF are preserved both in the hanging wall and footwall of the Alpine thrusts. The best outcrops where the LNF structure is observable are in the footwall, at the center of the map (yellow box).

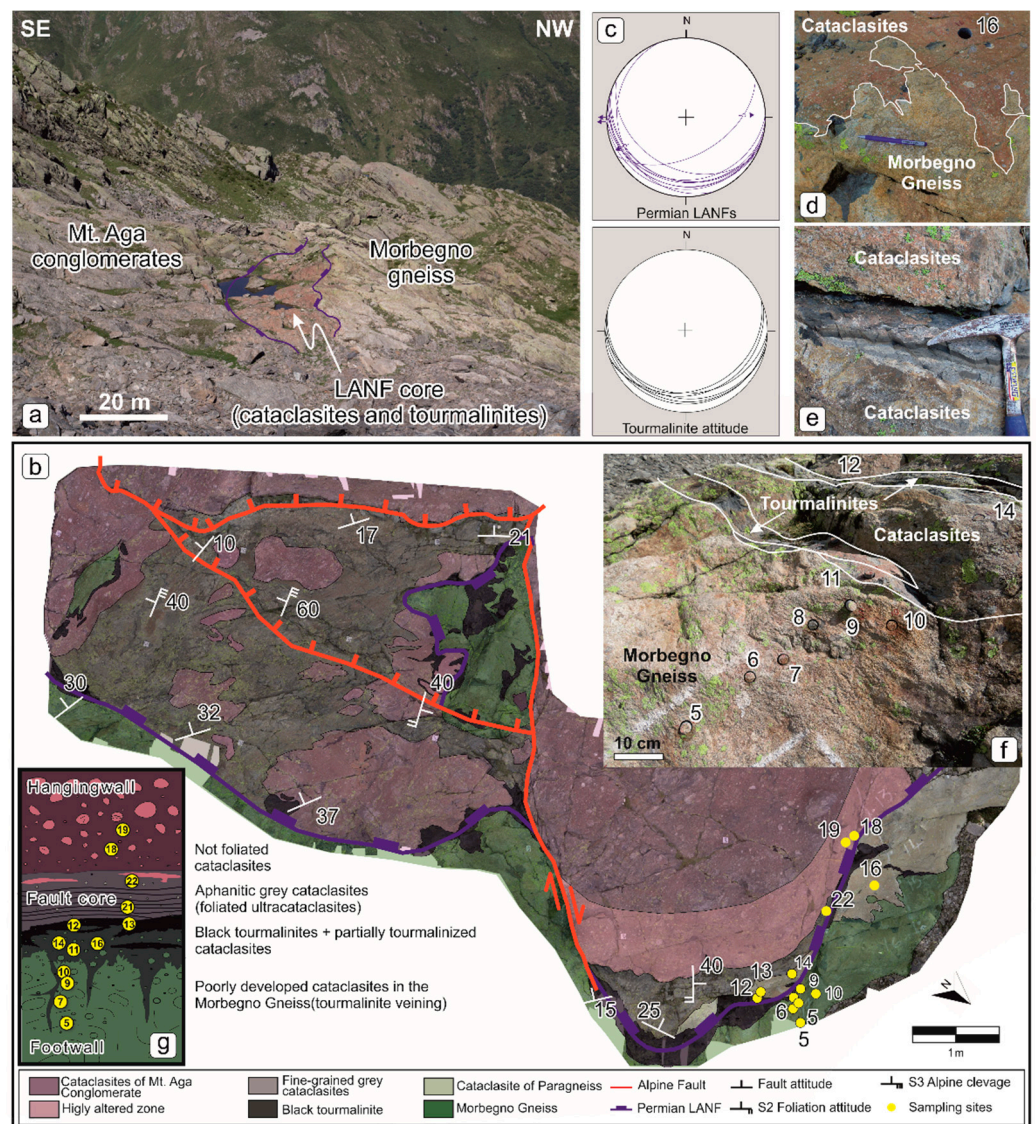


**Figure 4.** (a) The main outcrop viewed from the Forcellino Pass (see Figure 3 for location). (b) Detailed map of the outcrop exposing the preserved Permian fault structure. The map has been obtained from manual photogrammetric reconstruction of the outcrop. (c) Sketch of the LANF structure with sampling locations. (d) Attitude of tourmalinites layers and LANF slip planes. (e) The contact between crystalline basement and reddish cataclasites derived from the Mt. Aga conglomerates. (f) The typical banded texture of the fault core characterized by alternating black tourmalinites and gray cataclasites levels. (g) A detail of the sampling transect from the footwall through the fault core. (h) Image of the sampled transect from the basement footwall across the fault core. (i) Reconstruction of the fault structure with sampling locations.

The outcrop displaying the best exposure of the LANF surface was reconstructed through photogrammetry, as reported in Figure 4. The entire outcrop surface has been photographed with a digital reflex camera, with photos shot from a constant camera-outcrop distance of 120 cm. Overlapping between adjacent images was ca. 60%. The photogrammetric reconstruction was obtained with the Agisoft Photoscan software.

The mineral chemistry of tourmaline and tourmalinites was determined by a JEOL 8200 Superprobe equipped with five WDS (Wavelength Dispersive Spectrometers) at the Electron Microprobe Lab of the Earth Sciences Department of the University of Milan, Italy. Analytical conditions were as follows: 15 kV of accelerating potential, 5 nA of sample

current with a spot size of 3  $\mu\text{m}$ . Counting times for each analysis were 30 s on the peak and 10 s on the background. Natural oxides and silicates were used as standards. Tourmaline analyses were recalculated following the general formula  $\text{XY}_3\text{Z}_6(\text{BO}_3)_3\text{T}_6\text{O}_{18}\text{V}_3\text{W}$  with  $\text{X} = \text{Na, Ca, K}$ ;  $\text{Y} = \text{Mg, Fe}^{2+}, \text{Fe}^{3+}, \text{Li, Al, Mn, Ti}^{4+}, \text{Cr}^{3+}$ ;  $\text{Z} = \text{Al, Mg, Fe}^{3+}, \text{Cr}^{3+}$ ;  $\text{T} = \text{Si, Al}$ ;  $\text{V} = \text{OH, O}$ ;  $\text{W} = \text{OH, F, O}$  [53].  $\text{B}_2\text{O}_3$  and  $\text{H}_2\text{O}$  have not been measured, but have been recalculated based on stoichiometry, considering 3 B atoms per formula unit. Results are reported in Table S1.

### 3. Results

The bedrock in the study area belongs to the Variscan basement, here made of paragneiss (“Morbegno Gneiss” Auct.) and mica schists [38] (“Edolo Schists” Auct.) that in the Vedello valley are repeatedly alternating [38,54], with a predominance of two mica paragneisses. Lenses of leucocratic orthogneisses (“Corno Stella Gneiss” Auct.) of Ordovician intrusion age [53] occur in the western part of the study area, representing the footwall basement rocks of the MF and AVF LANFs (Figures 2 and 3). The peak metamorphic phase assemblage is made of quartz, plagioclase, biotite, white mica, garnet, staurolite, and kyanite [39], which were later retrogressed at greenschist facies conditions. Within paragneisses, the greenschist facies retrogression was accompanied by the growth of millimetric-sized periclinoblast of albitic plagioclase that gave the typical spotted aspect of the “Morbegno Gneiss” Auct.

The Upper Carboniferous to Lower Permian volcanic and volcanoclastic succession was deposited in non-conformity on the Variscan basement. The “Basal Conglomerate” Auct., consisting of sandstones and conglomerates with quartz and basement-derived clasts [25,27], occurs in the study area only in the upper Brembana Valley to the south of the Fregaborgia Fault (Figure 2). The lowermost parts of the Lower Permian succession deposited above the basement rocks along the Brembana-Vedello watershed and in the upper Vedello valley are the Monte Aga and Vedello conglomerates, belonging to the Pizzo del Diavolo Fm. [32]. Conglomerates consist of mainly sub-angular and minor sub-rounded pebbles up to several decimeters in size (Figure 5a). Garnet mica schists, two-mica paragneisses, and granitoid orthogneisses dominate the pebbles lithologies, with minor volcanoclastic pebbles occurring in the upper part of the successions, where the conglomerates progressively grade into sandstones.

The Variscan P-T evolution of the basement-derived pebbles of the Val Vedello and Aga conglomerates (Figure 2) are different. A first type (Type 1 [32]) is characterized by an amphibolite facies metamorphic imprint followed by greenschist facies re-equilibration; a second type (Type 2 [32]) displays, instead, three successive greenschist facies re-equilibrations. Comparisons with the metamorphic evolution of the Val Vedello basement pointed out that Type 1 pebbles are closely similar with their underlying basement, whereas greenschist facies pebbles likely derived from adjacent areas, mainly located to the east of Vedello Valley [32,39].

#### 3.1. Structural Analysis

##### 3.1.1. Mesostructural Features

At Lago del Diavolo and Mt. Masoni areas (Figure 1), the fault core of the Aga-Vedello LANF is well exposed, with several outcrops also displaying evidence of syn-tectonic sedimentation in the hanging wall (Figure 5c,d), as already outlined by other authors [8,25,33].

The same structure crops out in the Ambria and Vedello valleys (Figures 1 and 2). Despite the reactivation of the Aga-Vedello LANF during the Alpine shortening, several fault segments preserve the original Permian features and are still observable in the field.

In the Forcellino Pass area, a several meters-wide outcrop of the fault zone is nicely preserved and well exposed (Figure 4a), thanks to the glacier erosion that smoothed the outcrop surface. The outcrop where the fault zone structure is best exposed is about  $10 \times 7$  m (Figure 4a,b), the main plane attitude of the LANF surface in this area (Figure 4a)

dips to SSE, with a dip angle of  $5^{\circ}$ – $10^{\circ}$  (Figure 4c). The fault zone is characterized by 40–50 cm thick reddish cataclasites, mainly developed at the expense of conglomerates in the hanging wall with minor involvement of the footwall basement paragneisses (Figure 4d,e and Figure 6b).



**Figure 5.** (a) Field aspect of the Aga Conglomerate, with pebbles chiefly made of paragneiss, mica schists and polycrystalline quartz. (b) The typical banded texture of the “Morbegno Gneiss” rich in albite peciloblasts. Syn-sedimentary normal faults within volcaniclastic sandstones of the upper part of the Mt. Aga Conglomerates to the north (c) and southeast (d) of the Forcellino Pass. These faults show very similar features with the syn-sedimentary faults described in the nearby Cima Aga area (Figure 2) in the hanging wall of the same LANF [9]. (e) S-C structures developed within Aga conglomerates along the Alpine thrusts. (f) Alpine cleavage affecting a black tourmalinite layer within the fault core.

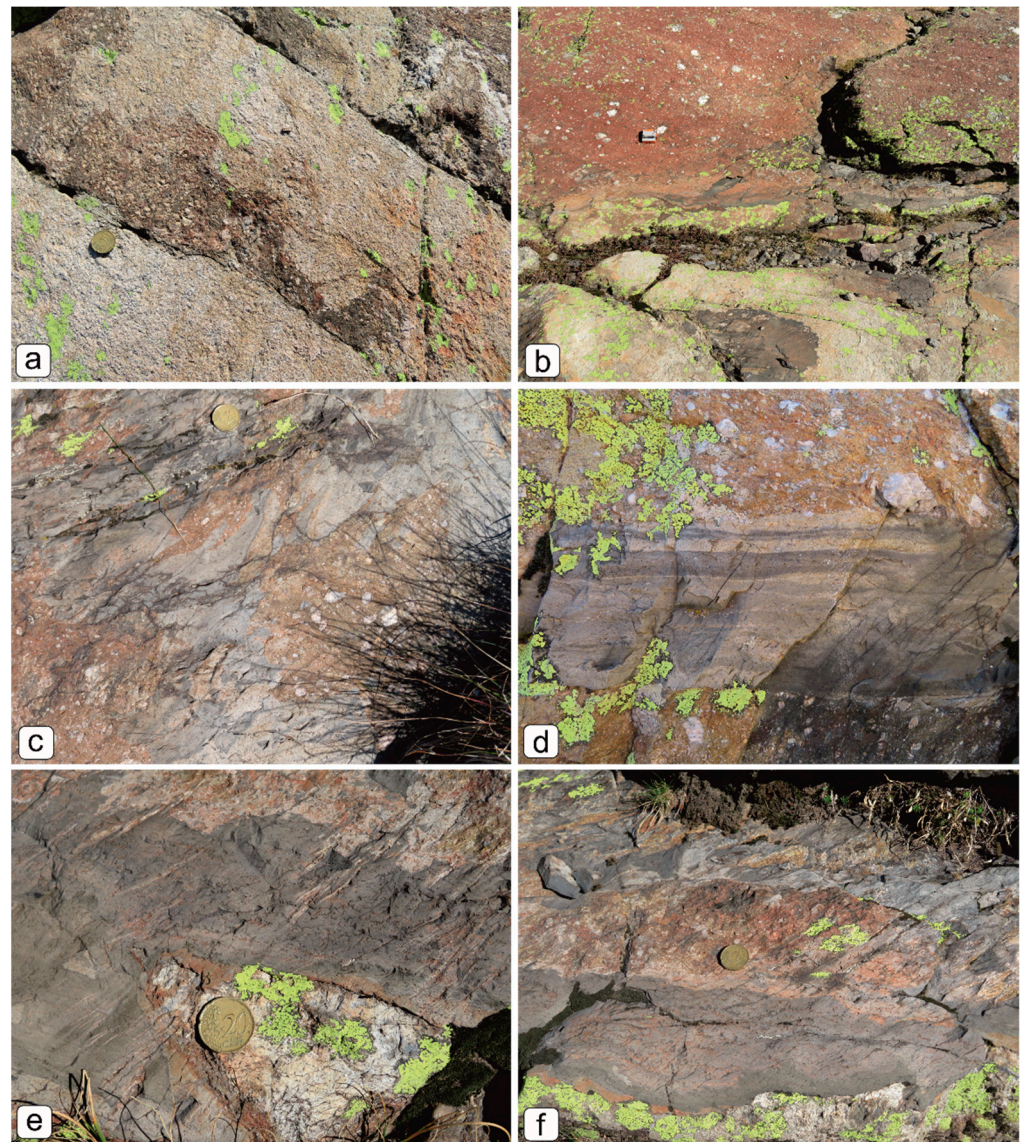


**Figure 6.** Field images of the main studied outcrop. (a) A tourmalinite vein propagated into the footwall paragneisses. (b) Reddish cataclasites after Mt. Aga Conglomerate with whitish quartz clast. They pass downward to gray cataclasites and black tourmalinites in contact with the footwall basement cataclasites. (c) Irregular contact between gray cataclasites/tourmalinites with the hosting reddish cataclasites, coin diameter is 22 mm. (d) Banded texture of tourmalinites with black levels made nearly entirely of tourmaline interleaved with gray-colored, partially tourmalinized cataclasites. (e) Alpine  $S_3$  cleavage (top-right to down left) developed within the LANF fault core, coin diameter is 22 mm. (f) Undulated contact between tourmalinites and the host rock, coin diameter is 22 mm.

Cataclasites are partially to completely substituted by tourmalinites. Field structural analysis suggests that tourmalinites seal the fault zone and maintain the same attitude of the LANF plane (Figure 4e), with only minor intrusion in the footwall as veins (Figure 6a). The Alpine deformation in the fault core and adjacent wall rocks unevenly resulted in the development of a non-pervasive slaty cleavage, mainly within fine-grained grey cataclasites (Figure 6e,f), but also within black tourmalinites (Figure 5f). The hanging wall is made of coarse-grained proximal conglomerates (Mt. Aga and Vedello conglomerate) with boulders of basement-derived gneisses and mica schists (Figure 5a), whereas the footwall consists of two mica gneisses with diffuse albite peciloblasts (Figure 5b).

The fault zone consists of reddish cataclasites and very fine-grained gray cataclasites (Figure 6). A banded texture is frequently developed with alternating black tourmalinite and partially tourmalinized grey cataclasites (Figure 6d). Cataclasites derived from paragneiss in the LANF's footwall are only partially tourmalinized, with cataclasis that is limited to the first 20–25 cm away from the first tourmalinite level in the fault core.

The size and amount of clasts in the tourmalinized cataclasites increase upward, displaying a gradual transition between tourmalinite and the overlying conglomerates (Figure 4b).

In the hanging wall of the LANF, away from the cataclastic zone and mainly within sandy layers of the Mt. Aga Conglomerate, syn-sedimentary high-angle Andersonian normal faults sparsely occur (Figure 5c,d and Figure 7e). These faults show centimeter-scale displacements associated with soft-sediment deformations developed during the sedimentation in non-consolidated sediments in hydroplastic conditions (Figure 5c,d). The occurrence of such structures in the hanging wall of the main LANFs surfaces has been already documented and discussed in the nearby area [9].

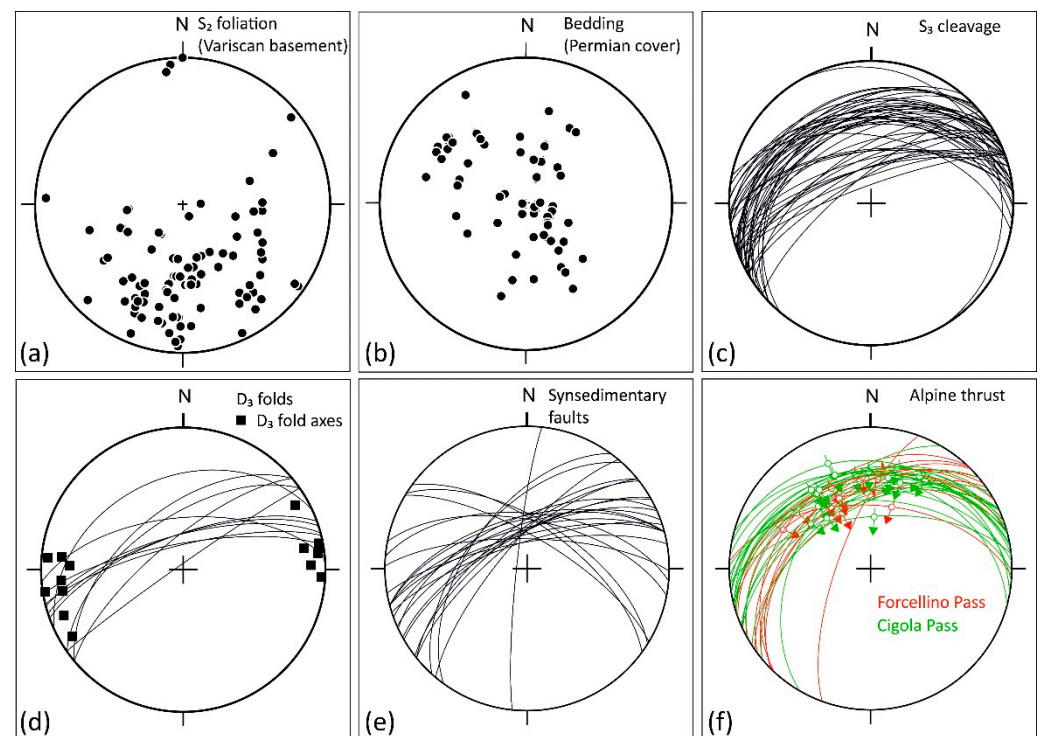


**Figure 7.** Stereographic projections (equal area, lower hemisphere) of mesoscopic structures in the Forcellino Pass area. (a) Poles to planes of the main foliation (S<sub>2</sub>) in the Variscan basement. (b) Poles to bedding planes in the Pizzo del Diavolo Fm. (c) S<sub>3</sub> axial plane cleavage of Alpine age in the hanging wall of the LANF. (d) Axial planes and fold hinges of D<sub>3</sub> folds, measured both in the crystalline basement and in the Permian cover. (e) Syn-sedimentary normal faults. (f) Fault slip data related to Alpine thrust at the Forcellino and Cigola passes.

The Alpine deformation, beside the previously described slaty cleavage in the fault zone, also consists of a more discrete to pervasive NNW dipping axial plane cleavage related to regional ENE-WSW trending folds (Figure 7c). Other main Alpine structures are thrust faults with top-to-S or top-to-SE kinematics (Figure 7f), associated with secondary splays at the Forcellino Pass (Figures 3 and 5e) and in the nearby Cigola Pass area (Figure 2). The fault zones associated with these thrusts range in thickness from ca. 50 to 150 cm. Foliated cataclasites with frequent S-C structures are the typical fault rocks (Figure 6e).

### 3.1.2. Microstructural Analysis

We sampled the LANF fault zone along a transect perpendicular to the fault plane (Figure 4) and with continuous exposure from the paragneisses in the footwall to the non-tourmalinized cataclasites in the hanging wall. The main purpose was to determine the microstructural and textural features across the fault core, in order to characterize the interactions of hydrothermal Boron-rich fluids with the fault rocks.

Microscopically, it is recognizable the action of hydrothermal fluids replacing the former rock with different intensities. The metasomatic event was likely successive to cataclasis since the passage of fluids modified the former cataclastic textures. The replacement is stronger in the “black tourmalinites” (e.g., sample FC12 and FC13, see samples position in Figure 4), as they are composed of more than 80% of dark microcrystalline tourmaline. Former cataclasites in the fault core were characterized by a very fine grain size which likely eased the chemical reaction between circulating fluids and both the cataclastic matrix and clasts, mainly consisting of polycrystalline quartz and plagioclase. This is documented by the rounded shape of the clasts and the occurrence of rim reactions on clasts displaying embayments (Figure 8a), representing the resorption of quartz clasts by hydrothermal fluids. On the other hand, moving from the fault core towards the hanging wall, cover-derived cataclastic rocks are characterized by higher clast/matrix ratio and larger clasts grain size (e.g., sample FC22, see the position in the sketch of Figure 4), suggesting a lower rate of replacement. The outcome is the production of very fine-grained to microcrystalline gray cataclasites, where the abundance of tourmaline in the matrix is lower and is usually associated with the presence of sericite. Rare single crystals of tourmaline occur usually within these gray cataclasites (Figure 8b).

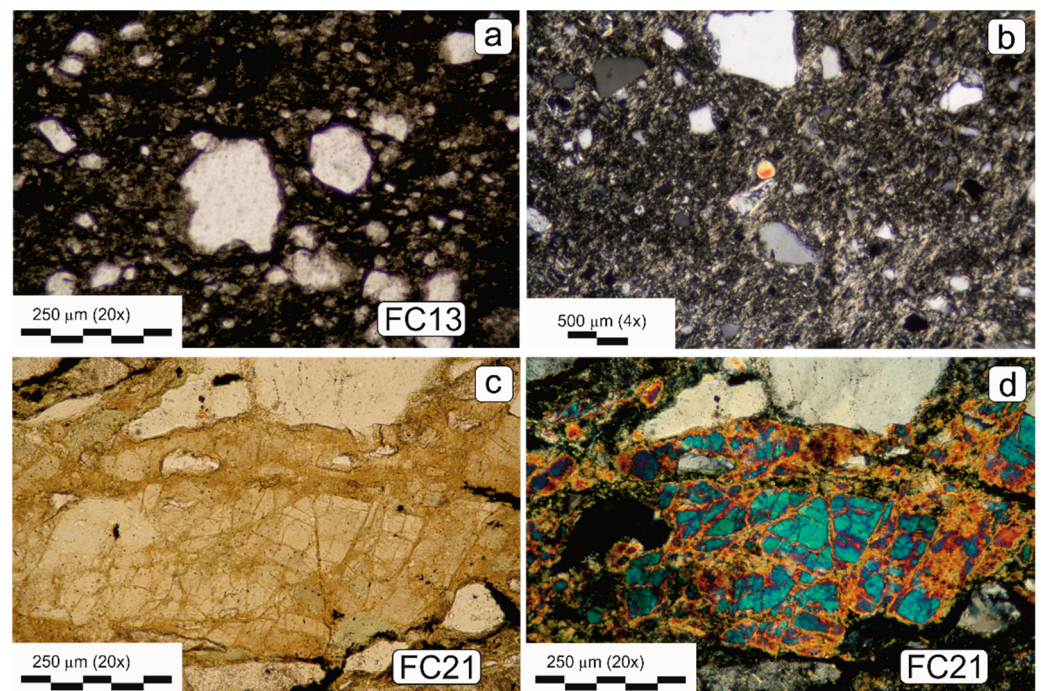


**Figure 8.** (a) Rounded quartz clasts in black tourmalinite of sample FC13. The rounded shape and the occurrence of embayments on larger clasts is a clue for chemical reaction between fluids and former cataclasite. (b) Microscopic aspect of a gray cataclasite (sample FC22); two crystals of tourmaline occur close to the center of the image. (c) Aggregate of light green, slightly pleochroic tourmaline crystals formed in a vein that branches out of the fault core into the footwall. The crystal aggregate has undergone weak cataclasis after its formation, as clearly visible in the cross-polarised image (d).

At Forcellino Pass, black tourmalinites represent the strongest effect of tourmalinization; however, there are other, less tourmalinized facies, especially in the basement, in which

the replacement by tourmaline commonly follows the main foliation planes, mylonitic bands in strained levels, and discordant fractures. The largest aggregates of tourmaline crystals  $> 50 \mu\text{m}$  in size were found (Figure 8c,d, sample FC21) along fractures branching from the fault core in the footwall.

Moving from the footwall through the fault core into the hanging wall, the microstructural features of fault rocks display several changes. Paragneiss of sample FC5 is mainly composed of quartz, plagioclase, white mica, chlorite, and accessory phases, such as ilmenite, apatite, and zircon (Figure 9a). Cataclastic plagioclase is frequently sericitized and the effect of metasomatism is recognizable due to the presence of carbonates and tourmalines, which are distinguishable in single green-brown crystals or aggregates. The secondary replacement of original mineralogical phase assemblage is confined along high-strain zones, usually localized at the microscopic scale around rigid polycrystalline quartz-plagioclase aggregates (e.g., sample FC9, Figure 9b).

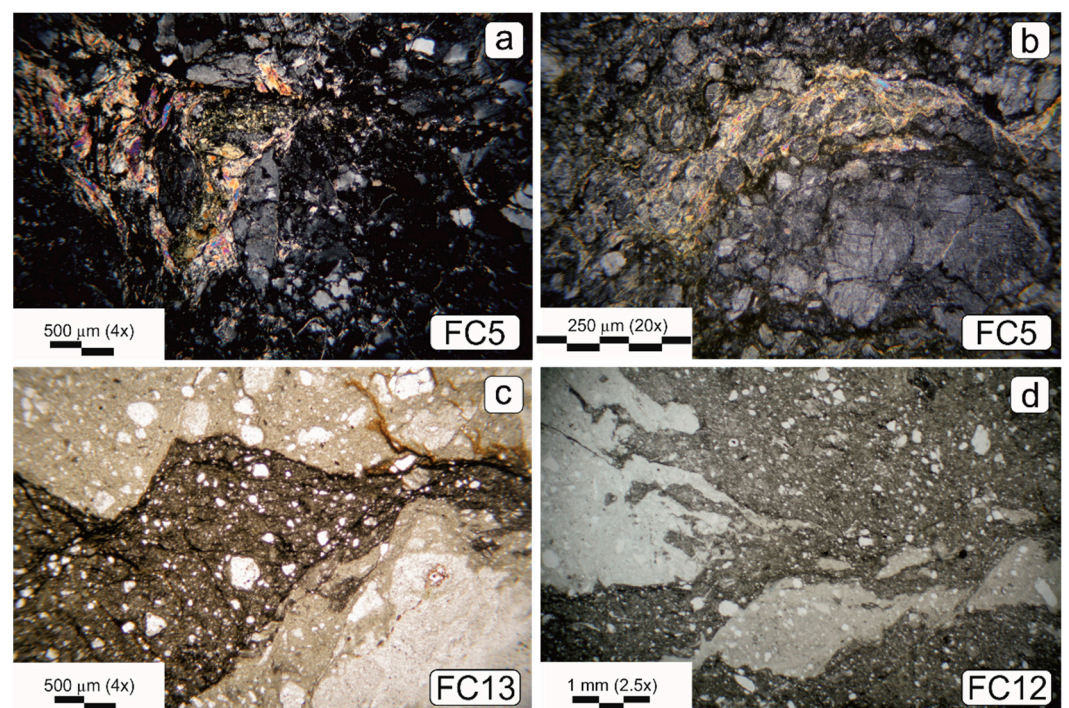


**Figure 9.** (a) Cataclastic paragneiss with partial tourmalinization. Tourmaline crystals occur in aggregates together with sericite (sample FC5). (b) Cataclastic quartz and plagioclase surrounded by sericitic aggregates containing a few tourmaline crystals. (c) The effect of tourmalinization in conglomerates-derived cataclasites (sample FC13): the original light-brown cataclasite matrix is substituted by a darker one with aphanitic tourmalinite black seams. Note the reduction in clasts grain size due to chemical reabsorption. (d) The effect of Boron-metasomatism on former cataclasites is inhomogeneous not only at the outcrop scale, but also at the microscopic scale. Light-colored cataclasites are preserved as millimetric domains within dark-colored tourmalinized cataclasites (sample FC12).

The relative chronology among cataclasites and tourmalinization clearly emerges from the microstructural features. Tourmalinites replace cataclasites along irregular veins where the metasomatic effect is not pervasive (Figure 9c, sample FC13). Where the metasomatic effect is more intense, pre-existing cataclasites are preserved only as small relict domains within black tourmalinites (Figure 9d). The black tourmalinites in the fault core are texturally homogeneous with a microcrystalline tourmaline matrix that embeds from 10 to 30% of fine-grained quartz clasts. The gray cataclasites flanking the fault core are instead characterized by the alternating layers more or less rich in tourmaline, which is more abundant in dark-colored layers. Moving in the hanging wall away from the fault core,

cataclasites derived from the Mt. Aga Conglomerate display an increasing clast/matrix ratio and finally grade into undeformed conglomerates.

Based on the observed microstructures, we can summarize that tourmaline occurs along the LANF fault zone in three distinct forms: (i) cryptocrystalline in the black tourmalinite matrix, (ii) as single crystals, especially in aphanitic gray cataclasites, (iii) as crystal aggregates in veins within the gneissic basement (e.g., sample FC21, Figure 7c,d).

### 3.2. Chemical Composition of Tourmaline

All crystal of tourmaline from the Forcellino Pass area display ( $Fe_{tot}/(Fe_{tot} + Mg)$ ) values in the 0.25–0.60 range (see Table S1 for microprobe analyses), combined with an X-site vacancy ratio of 0.10–0.35 (Figure 10a). All of them classify in the alkali group [55] based on cations proportions in the X-site (Figure 10c). The plot in the middle of the schorlite-dravite join on the Al-Mg-Fe diagram [55], within the field of typical tourmaline composition in metapelitic-metapsammitic rocks (Figure 10b).

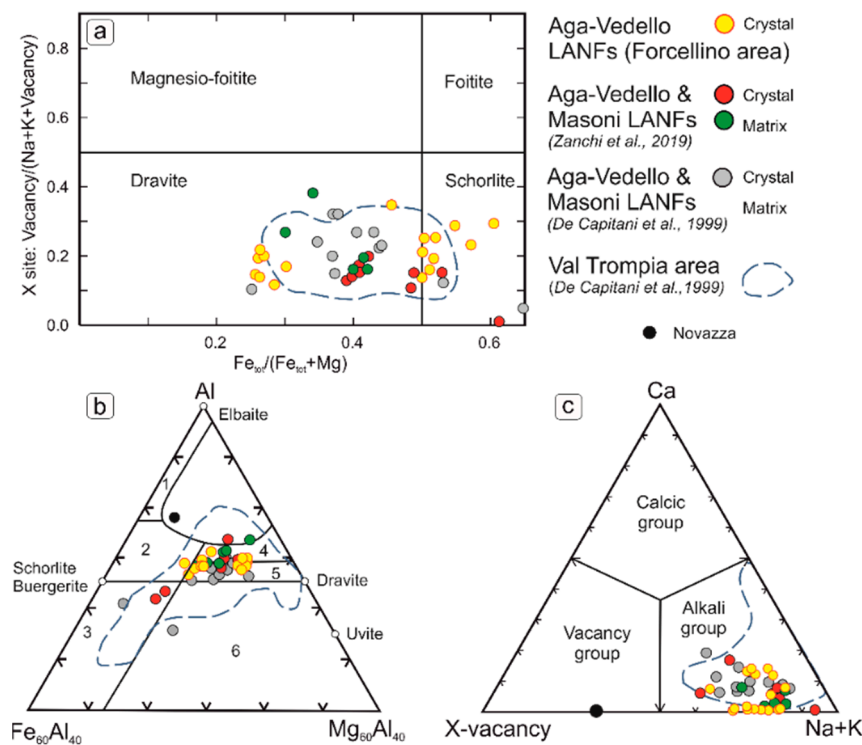


**Figure 10.** (a)  $xFe$  vs X-site alkali occupancy diagram: all analysed tourmaline and tourmalinites plot below the foitite-dravite divide. Tourmalines from the Forcellino Pass area display a clear zoning with Mg-rich cores and Fe-rich rims. The dashed blue line indicates the compositional field of tourmaline from the Trompia Valley area. (b) Fe-Mg-Al diagram [55]. The compositions are within field 4 and 5, typical of tourmalinites in metapelitic and metapsammitic rocks. (c) Classification diagram based on the principal constituent at the X-site [53]; all tourmalines from all the considered areas plot within the Alkali group field.

Analyzed tourmaline crystals from the Forcellino and Mt. Aga area tourmalinites (Figure 2) display a systematic Fe-enrichment from core to rim, with major compositional zoning in terms of Fe/Mg ratio observed in the Forcellino tourmalines, whereas the ones from the Mt. Aga and Masoni LANFs display minor compositional zoning with crystal cores and Mg-poor cores ( $Fe/(Fe + Mg)$  of 0.4), with respect to the Forcellino ones (Figure 10a).

Opposite to the Fe core-rim distribution is the Ca zoning. Ca is systematically lower than 0.05 apfu at cores while increasing up to ca. 0.14 at rims (Table S1). The alkaline nature of the Forcellino Pass tourmaline is largely controlled by the Na-content, which ranges from 0.67 to 0.84 apfu, with higher values shown in the crystal rims (Table S1). The only

other element that displays valuable core-rim zoning is Ti, with higher contents at cores (0.05–0.09 apfu) and lower at rims (0.02–0.05) (Table S1).

#### 4. Discussion and Conclusions

The Early Permian basins of the cSA developed within an intra-continental setting [27], characterized by tectonically-controlled evolution. Fault systems made of an association of Low-Angle-Normal-Faults (LANFs) and High-Angle-Normal-Faults (HANFs) controlled the tectonic and sedimentary evolution of these basins [9]. The Early Permian fault system, despite the Alpine shortening, is still well recognizable in several areas of the cSA [8,25,27]. One of these best-preserved Permian faults is the Aga-Vedello (AVF) LANF, extending for about 5–6 km across the Orobic Alps watershed (Figure 1, see also figures and tectonic model in [9]). The WSW-ENE trending AVF brings in contact the Variscan basement of the cSA with the Lower Permian succession of the Pizzo del Diavolo Fm., made of volcanic and volcanoclastic deposits [27]. The main fault plane gently (10–15°) dips to the south and can be followed from the Lago del Diavolo area into the Vedello Valley for at least 5 km (Figure 1). The occurrence of syndepositional tectonic structures in the hanging wall of the AVF LANF suggests that the fault was active during the opening of the Orobic Basin, together with growth faults and high-angle normal faults [9]. The same syndepositional structures also point to a shallow depth of activity for the LANF.

The occurrence of tourmalinites along Permian faults that controlled the opening of the Orobic Basin was reported by [33,34] in the Lago del Diavolo area and by [35], also in the Trompia Valley area, about 40 km to the SE of the Forcellino Pass. In this area, late Paleozoic–Early Permian intrusive bodies ranging in composition from granites to gabbros [56] intruded the Variscan basement. Tourmaline breccias are here typically associated with S-W-bearing ore deposits [35,51]. Several stages of tourmaline crystallization have been individuated, mainly based on textural differences and crystal zoning in terms of chemical composition [35]. At least four stages of crystallization have been recognized, with an increasing Fe/Mg ratio from stage (i) to stage (iv). From the textural features and observed chemical composition and zoning, the Trompia Valley tourmalinites have been considered to be of metasomatic origin, formed after the reaction between magmatic-hydrothermal fluids with the host rocks. Tourmalinites occur mainly along LANFs, but a remobilization of tourmalinites due to Alpine tectonics has been documented in the Vedello Valley area [31], with tourmalinites that have been described also along re-activated faults during the Alpine orogenesis. Tourmalinites mainly occur along LANFs as they represent the first highly permeable pathways that Boron-rich fluids encountered during their ascent. Tourmalinites of the Trompia Valley area occur as brecciated bodies roughly aligned along a major regional fault (the Val Trompia Line [35]) that likely acted as a preferred pathway for fluids migration. The chemical compositions of the Forcellino area tourmalinites closely match ones of the Trompia Valley area, falling within the Schorlite and Dravite compositional fields (Figure 10b). In terms of chemical zonation, they display the same Fe-enrichment trend (Figure 10a), with a difference in terms of  $Fe_{tot}/(Fe_{tot} + Mg)$  of ca 0.30 between cores and rims. Based on these similarities we can argue that the tourmalinites along the AVF LANF originated from Boron-rich fluids derived from crystallizing magmatic bodies, in a similar way to what was proposed for tourmalinites of the Trompia Valley area [35]. Conclusive evidence for this hypothesis is, however, still lacking.

Tourmalinites along the AVF LANF are the nearest to the Vedello Valley Uranium ore deposits. Here, the Uranium mineralization is concentrated along the Variscan basement-Permian deposits contact, i.e., along the NE prosecution of the AVF LANF. The ore genesis of the Vedello Uranium deposit has since been considered of hydrothermal origin, with a primary disseminated mineralization contained within several levels of the Monte Cabianna ignimbrites in the Novazza ore deposit [25]. The occurrence of Uranium-bearing ores in the Vedello Valley has been interpreted as a remobilization due to a late Permian–Early Triassic geothermal event that leached Uranium from the Lower Permian ignimbrites and transported it along existing faults with final concentration and deposition along the basement-

cover contact in the Vedello area [30,31]. Available ages of Uraninite and other Uranium-bearing mineral suggest an age of the Vedello Uranium deposit of  $275 \pm 13$  Ma [57]. The major proof of fluids circulation along Permian faults in the study area are tourmalinites, which have been already proposed [34] to be correlated to the formation of the U-Zn Vedello ores. The tourmalinites that have since been studied crop out in the Trompia Valley area [35] and the Lago del Diavolo–Lago del Publino area (Figure 1) [33–35]. The outcrop of the Forcellino Pass is the closest to the Vedello Uranium deposit and thus represents the best opportunity to investigate the possible relationships between the tourmalinization phenomena and the genesis of the U-Zn ores. The age of the Uranium mineralization in the Novazza mine has been constrained at  $275 \pm 13$  Ma [57]; these last data were obtained from microchemical dating of uraninite within a siderite vein. Younger ages have been obtained for the Vedello ores, ranging between 200 and 50 Ma [31,57]. The large time span and the young ages of the Vedello uraninites have been attributed to remobilization and recrystallization of Uranium minerals during the Alpine tectonic activity, considering the primary U-mineralization coeval to the Novazza one. The ages of the intrusives and volcanics that represent Uranium source rocks in the above-described model are constrained to  $280 \pm 2.5$  Ma for the basal tuff of the Monte Cabbianca ignimbrites [45]. Similar ages have been proposed for the Trompia Valley granitoids, 271–274 Ma [56], obtained on magmatic biotite and whole rock with the Rb-Sr method, so considered to be minimum intrusion ages.

The wealth of geological and geochronological data strongly suggests that the metasomatism operated by Boron-rich fluids that circulated along the Permian fault system [9,25] was coeval with the Early Permian magmatic activity that occurred in the central Southern Alps domain. Early Permian magmatic rocks are thus ideal candidates for Uranium pristine source, both for late-stage magmatic fluids that leached and later concentrated Uranium in the Novazza and Vedello mining districts. In the Lago del Diavolo and Forcellino Pass areas, tourmaline metasomatism postdated the main activity of the Permian fault systems responsible for the opening of the Orobic Basin. The effects of Boron-rich fluids circulation promoted the metasomatism of pre-existing cataclasites indicating that tourmalinization occurred after or in the latest stage of faults activity. A direct correlation with the circulation of hydrothermal Boron-rich fluids with Uranium leaching from the Permian volcanic rocks and its concentration and deposition in the Vedello ores is still under investigation, but the occurrence of tourmalinites in the same area and the same structural position, i.e., along Low-Angle Normal Faults, strongly suggests a connection between the two.

**Supplementary Materials:** The following are available online at <https://www.mdpi.com/article/10.3390/min12040404/s1>, Table S1: Chemical composition of tourmalines from the Forcellino Pass area.

**Author Contributions:** Conceptualization, S.Z. and A.Z.; methodology, S.Z.; validation, S.Z., S.L., C.M. and A.Z.; investigation, S.Z., S.L., G.C. and M.M.; resources, S.Z. and A.Z.; data curation, S.Z. and S.L.; writing—original draft preparation, S.L. and S.Z.; writing—review and editing, S.Z., S.L., A.Z. and C.M.; supervision, A.Z.; funding acquisition, S.Z. and A.Z. All authors have read and agreed to the published version of the manuscript.

**Funding:** This research was funded by “The University of Milano Bicocca, grant number 2019-ATE-0039” awarded to S.Z.

**Acknowledgments:** M. Roda and two anonymous reviewers are warmly thanked for providing critical comments and suggestions on a first draft of this paper.

**Conflicts of Interest:** The authors declare no conflict of interest.

## References

1. Brodie, K.H.; Rex, D.; Rutter, E.H. On the age of deep extensional crustal faulting in the Ivrea Zone, Northern Italy. In *Alpine Tectonics*; Coward, M.P., Dietrich, D., Park, R.G., Eds.; Geological Society, London, Special Publications: London, UK, 1989; Volume 45, pp. 203–210.
2. Diella, V.; Spall, M.L.; Tunesi, A. Contrasted thermomechanical evolutions in the Southalpine metamorphic basement of the Orobic Alps (Central Alps, Italy). *J. Metamorphic. Geol.* **1992**, *10*, 203–219. [[CrossRef](#)]

3. Handy, M.R.; Franz, L.; Heller, F.; Janott, B.; Zurbriggen, R. Multistage accretion and exhumation of the continental crust (Ivrea crustal section, Italy and Switzerland). *Tectonics* **1999**, *18*, 1154–1177. [[CrossRef](#)]
4. Berra, F.; Carminati, E. Subsidence history from a backstripping analysis of the Permo-Mesozoic succession of the Central Southern Alps (Northern Italy). *Basin Res.* **2009**, *22*, 952–975. [[CrossRef](#)]
5. Bernoulli, D.; Winkler, W. Heavy mineral assemblages from South- and Austroalpine Flysch sequences (Northern Italy and Southern Switzerland). Source terranes and paleotectonic implications. *Eclogae Geol. Helv.* **1990**, *83*, 287–310.
6. Bertotti, G.; Picotti, V.; Bernoulli, D.; Castellarin, A. From rifting to drifting: Tectonic evolution of the South-Alpine upper crust from the Triassic to the Early Cretaceous. *Sediment. Geol.* **1993**, *86*, 53–76. [[CrossRef](#)]
7. Blom, J.C.; Passchier, C.W. Structures along the Orobic thrust, Central Orobic Alps, Italy. *Geol. Rundsch.* **1997**, *86*, 627–636. [[CrossRef](#)]
8. Zanchetta, S.; Malusà, M.; Zanchi, A. Precollisional development and Cenozoic evolution of the Southalpine retrobelt (European Alps). *Lithosphere* **2015**, *7*, 662–681. [[CrossRef](#)]
9. Zanchi, A.; Zanchetta, S.; Berio, L.; Berra, F.; Felletti, F. Low-angle normal faults record Early Permian extensional tectonics in the Orobic Basin (Southern Alps, N Italy). *Ital. J. Geosci.* **2019**, *138*, 184–201. [[CrossRef](#)]
10. Froitzheim, N.; Derks, J.F.; Walter, J.M.; Sciunnach, D. Evolution of an Early Permian extensional detachment fault from synintrusive, mylonitic flow to brittle faulting (Grassi Detachment Fault, Orobic Anticline, southern Alps, Italy). In *Tectonic Aspects of the Alpine-Dinaride-Carpathian System*; Siegesmund, S., Fugenschuh, B., Froitzheim, N., Eds.; Geological Society, London, Special Publications: London, UK, 2008; Volume 298, pp. 69–82. [[CrossRef](#)]
11. Pohl, F.; Froitzheim, N.; Obermüller, G.; Tomaschek, F.; Schroder, O.; Nagel, T.J.; Sciunnach, D.; Heuser, A. Kinematics and Age of Syn-Intrusive Detachment Faulting in the Southern Alps: Evidence for Early Permian Crustal Extension and Implications for the Pangea A Versus B Controversy. *Tectonics* **2018**, *37*, 3668–3689. [[CrossRef](#)]
12. Arthaud, F.; Matte, P. Late Paleozoic strike-slip faulting in southern Europe and northern Africa: Result of a right-lateral shear zone between the Appalachians and the Urals. *Geol. Soc. Am. Bull.* **1977**, *88*, 1305–1320. [[CrossRef](#)]
13. Rebay, G.; Spalla, M.I. Emplacement at granulite facies conditions of the Sesia-Lanzo metagabbros: An early record of Permian rifting? *Lithos* **2001**, *58*, 85–104. [[CrossRef](#)]
14. Schaltegger, U.; Brack, P. Crustal-scale magmatic systems during intracontinental strike-slip tectonics: U, Pb and Hf isotopic constraints from Permian magmatic rocks of the Southern Alps. *Int. J. Earth Sci.* **2007**, *96*, 1131–1151. [[CrossRef](#)]
15. Spalla, M.I.; Zanoni, D.; Marotta, A.M.; Rebay, G.; Roda, M.; Zucali, M.; Gosso, G. *The Transition from Variscan Collision to Continental Break-Up in the Alps: Insights from the Comparison between Natural Data and Numerical Model Predictions*; Geological Society, London, Special Publication: London, UK, 2014; Volume 405, pp. 363–400. [[CrossRef](#)]
16. Schuster, R.; Stüwe, K. Permian metamorphic event in the Alps. *Geology* **2008**, *36*, 603–606. [[CrossRef](#)]
17. Marotta, A.M.; Spalla, M.I.; Gosso, G. *Upper and Lower Crustal Evolution during Lithospheric Extension: Numerical Modelling and natural Footprints from the European Alps*; Geological Society, London, Special Publication: London, UK, 2009; Volume 321, pp. 33–72.
18. Sinigoi, S.; Quick, J.E.; Clemens-Knott, D.; Mayer, A.; Demarchi, G.; Mazzuchelli, M.; Negrini, L.; Rivalenti, G. Chemical evolution of a large mafic intrusion in the lower crust, Ivrea-Verbano Zone, northern Italy. *J. Geophys. Res.* **1994**, *B11*, 575–590. [[CrossRef](#)]
19. Zingg, A. The Ivrea and Strona-Ceneri zones (Southern Alps, Ticino and N-Italy)—A review. *Schweiz. Miner. Petrogr. Mitteilungen* **1983**, *63*, 361–392.
20. Müntener, O.; Hermann, J.; Trommsdorff, V. Cooling history and exhumation of lower crustal granulite and upper mantle (Malenco, Eastern Central Alps). *J. Petrol.* **2000**, *41*, 175–200. [[CrossRef](#)]
21. Tribuzio, R.; Thirlwall, M.F.; Messiga, B. Petrology, mineral and isotope geochemistry of the Sondalo gabbroic complex (Central Alps, Northern Italy): Implications for the origin of post-Variscan magmatism. *Contrib. Mineral. Petrol.* **1999**, *136*, 48–62. [[CrossRef](#)]
22. Rottura, A.; Bargossi, G.M.; Caggianelli, A.; Del Moro, A.; Visonà, D.; Tranne, C.A. Origin and significance of Permian high-K calc-alkaline magmatism in the central-eastern Southern Alps, Italy. *Lithos* **1998**, *45*, 329–348. [[CrossRef](#)]
23. Steck, A.; Della Torre, F.; Keller, F.; Pfeifer, H.R.; Hunziker, J.; Masson, H. Tectonics of the Lepontine Alps: Ductile thrusting and folding in the deepest tectonic levels of the Central Alps. *Swiss. J. Geosci.* **2013**, *106*, 427–450. [[CrossRef](#)]
24. Bergomi, M.; Dal Piaz, G.V.; Malusà, M.G.; Monopoli, B.; Tunesi, A. The Grand St Bernard-Briançonnais Nappe System and the Paleozoic Inheritance of the Western Alps Unraveled by Zircon U-Pb Dating. *Tectonics* **2017**, *36*, 2950–2972. [[CrossRef](#)]
25. Cadel, G.; Cosi, M.; Pennacchioni, G.; Spalla, M.I. A new map of the Permo-Carboniferous cover and Variscan metamorphic basement in the Central Orobic Alps, Southern Alps-Italy: Structural and stratigraphical data. *Mem. Sci. Geol.* **1996**, *48*, 1–53.
26. Cortesogno, L.; Cassinis, G.; Dallagiovanna, G.; Gaggero, L.; Oggiano, G.; Ronchi, A.; Seno, S.; Vanossi, M. Carboniferous-Permian sequences of Ligurian Alps, Southern Alps and Sardinia (Italy): A synthesis. *Lithos* **1998**, *593*, 1–19.
27. Berra, F.; Felletti, F.; Tessarollo, A. Stratigraphic architecture of a transtensional continental basin in low-latitude semi-arid conditions: The Permian succession of the central Orobic Basin (Southern Alps, Italy). *J. Sediment. Res.* **2016**, *86*, 408–429. [[CrossRef](#)]
28. Cassinis, G.; Perotti, C.; Ronchi, A. Permian continental basins in the Southern Alps (Italy) and peri-mediterranean correlations. *Int. J. Earth Sci.* **2012**, *101*, 129–157. [[CrossRef](#)]

29. Sciunnach, D. Early Permian paleofaults at the western boundary of the Collio Basin (Valsassina, Lombardy). In *Permian Continental Deposits of Europe and Other Areas. Regional Reports and Correlations*; Museo Civico di Scienze Naturali di Brescia: Brescia, Italy, 2001; pp. 37–43.
30. Dal Piaz, G.V.; Eusebio, A.; Gosso, G.; Martinotti, G.; Massari, F.; Milano, P.F.; Pennacchioni, G.; Perello, M.; Pessina, C.M.; Roman, E.; et al. Report on a structural and sedimentological analysis in the Uranium province of the Orobic Alps, Italy. *Uranium* **1986**, *2*, 241–260.
31. Philippe, S.; Villemaire, C.; Lancelo, J.R.; Girod, M.; Mercadier, H. Données minéralogique et isotopiques sur deux gîtes hydrothermaux uranifères du bassin volcano-sédimentaire permien de Collio Orobico (Alpes Bergamasques): Mise en évidence d’une phase de remobilisation crétacée. *Bull. Miner.* **1987**, *110*, 283–303. [[CrossRef](#)]
32. Zanoni, D.; Spalla, M.I.; Gosso, G. Vestiges of lost tectonics units in conglomerate pebbles? A test in Permian sequences of the Southalpine Orobic Alps. *Geol. Mag.* **2010**, *147*, 98–122. [[CrossRef](#)]
33. Zhang, J.S.; Passchier, C.W.; Slack, J.F. Cryptocrystalline Permian tourmalinites of possible metasomatic origin in the Orobic Alps, Northern Italy. *Econ. Geol.* **2010**, *89*, 391–396. [[CrossRef](#)]
34. Slack, J.F.; Passchier, C.W.; Zhang, J.S. Metasomatic tourmalinite formation along basement-cover décollements, orobic Alps, Italy. *Schweiz. Miner. Petrogr. Mitt.* **1996**, *76*, 193–207.
35. De Capitani, L.; Moroni, M.; Rodeghiero, F. Geological and geochemical characteristics of Permian tourmalinization at Val Trompia (southern Alps, northern Italy) and relationship with the Orobic tourmalinites. *Period. Miner.* **1999**, *68*, 185–212.
36. Schönborn, G. Alpine tectonics and kinematic models of the central Southern Alps. *Mem. Sci. Geol.* **1992**, *44*, 229–393.
37. Carminati, E.; Siletto, G.B.; Battaglia, D. Thrust kinematics and internal deformation in basement-involved fold and thrust belts: The eastern Orobic Alps case (Central Southern Alps, northern Italy). *Tectonics* **1997**, *16*, 259–271. [[CrossRef](#)]
38. Milano, P.F.; Pennacchioni, G.; Spalla, M.I. Alpine and pre-Alpine tectonics in the Central Orobic Alps (Southern Alps). *Eclogae Geol. Helv.* **1988**, *81*, 273–293.
39. Spalla, M.I.; Gosso, G. Pre-Alpine tectonometamorphic units in the central Southern Alps: Structural and metamorphic memory. *Mem. Sci. Geol.* **1999**, *51*, 221–229.
40. Carminati, E.; Siletto, G.B. The Central Southern Alps (N. Italy) paleoseismic zone: A comparison between field observations and predictions of fault mechanics. *Tectonophysics* **2005**, *401*, 179–197. [[CrossRef](#)]
41. Brack, P. Structures in the southwestern border of the Adamello intrusion (Alpi bresciane, Italy). *Schweiz. Miner. Petrogr. Mitt.* **1981**, *61*, 37–50.
42. Fantoni, R.; Bersezio, R.; Forcella, F. Alpine structure and deformation chronology at the Southern Alps-Po Plain border in Lombardy. *Boll. Soc. Geol. Ital.* **2004**, *123*, 463–476.
43. Zanchetta, S.; D’Adda, P.; Zanchi, A.; Barberini, V.; Villa, I.M. Cretaceous-Eocene compressions in the central Southern Alps (N Italy) inferred from <sup>40</sup>Ar/<sup>39</sup>Ar dating of pseudotachylytes along regional thrust faults. *J. Geodyn.* **2011**, *51*, 245–263. [[CrossRef](#)]
44. D’Adda, P.; Zanchetta, S. Geological-structural map of the Orobic and Porcile thrust junction, central Southern Alps (N Italy). *J. Maps* **2015**, *11*, 25–38. [[CrossRef](#)]
45. Berra, F.; Tiepolo, M.; Vaironi, V.; Siletto, G.B. U-Pb zircon geochronology of the volcanic deposits from the Permian basin of the Orobic Alps (Southern Alps, Lombardy): Chronostratigraphic and geological implications. *Geol. Mag.* **2015**, *152*, 429–443. [[CrossRef](#)]
46. Petti, F.M.; Bernardi, M.; Ashley-Ross, M.A.; Berra, F.; Tessarollo, A.; Avanzini, M. Transition between terrestrial-submerged walking and swimming revealed by Early Permian amphibian trackways and a new proposal for the nomenclature of compound trace fossil. *Palaeogeogr. Palaeoclimatol. Palaeoecol.* **2014**, *410*, 278–289. [[CrossRef](#)]
47. Marchetti, L.; Tessarollo, A.; Felletti, F.; Ronchi, A. Tetrapod footprint paleoecology: Behavior, taphonomy and ichnofauna disentangled. A case study from the European Alps. *Palaios* **2017**, *32*, 506–527. [[CrossRef](#)]
48. Casati, P.; Gnaccolini, M. Geologia delle Alpi Orobic occidentali. *Riv. Ital. Paleobiol. Stratigr.* **1967**, *73*, 25–162.
49. Berra, F.; Felletti, F. Syndepositional tectonics recorded by soft-sediment deformation and liquefaction structures (continental Lower Permian sediments, Southern Alps, Northern Italy): Stratigraphic significance. *Sediment. Geol.* **2011**, *235*, 249–263. [[CrossRef](#)]
50. Frizzo, P. Le mineralizzazioni a fluorite e metalli della Val Trompia. In Proceedings of the Atti Della Giornata di Studio “Le Vene Delle Montagne”, Brescia, Italy, 24 November 1995.
51. Moroni, M. Identification of W-Sn mineralization associated with boron metasomatism in the crystalline basement of the Southern Italian Alps: Preliminary observations on a new finding. *Chron. Rech. Min.* **1994**, *514*, 38–43.
52. Cassinis, G.; Frizzo, P.; Moroni, M.; Rodeghiero, F. Le mineralizzazioni delle Alpi Bresciane: Aspetti geologico-minerari e metallogenici. In Proceedings of the Atti Della Giornata di Studio “Le Vene Delle Montagne”, Brescia, Italy, 24 November 1995.
53. Hawthorne, F.C.; Henry, D.J. Classification of the minerals of the tourmaline group. *Eur. J. Miner.* **1999**, *11*, 201–215. [[CrossRef](#)]
54. Bergomi, M. Integrated study of the “Gneiss Chiari” in the framework of the Orobic basement of Southern Alps (field relationships, mineral chemistry, geochemistry and geochronology). *Eur. J. Miner. Plinius Ital. Suppl.* **2004**, *30*, 54–59.
55. Henry, D.J.; Guidotti, C.V. Tourmaline as a petrogenetic indicator mineral: An example from the staurolite-grade metapelites of NW Maine. *Am. Miner.* **1985**, *70*, 1–15.

- 
56. De Capitani, L.; Delitala, G.; Liborio, G.; Mottana, A.; Rodeghiero, F.; Thoeni, M. The granitoid rocks of Val Navazze, Val Torgola and Val di Rango (Val Trompia, Lombardy, Italy). *Mem. Sci. Geol.* **1994**, *46*, 329–343.
  57. Martin, S.; Toffolo, L.; Moroni, M.; Montorfano, C.; Secco, L.; Agnini, C.; Nimis, P.; Tumiati, S. Siderite deposits in northern Italy: Early Permian to Early Triassic hydrothermalism in the Southern Alps. *Lithos* **2017**, *284–285*, 276–295. [[CrossRef](#)]